Research Article | DOI:10.5281/zenodo.18063772
www.jnanosam.com

NANOSAM
Journal of NanoScience in Advanced Materials

Investigation of Structural and Electrical Properties of 90%$La_{0.67}Pb_{0.33}MnO_3$ + 10%A and 90%$La_{0.67}Pb_{0.33}CoO_3$ + 10%A (A= MnO_2, NiO, SnO_2 and Cu_2O) Composite Materials

Barış Altan[1#], Ece Naz Özgün[2] and Esra Nur Bakay[2]

In this study, the crystal structures, surface morphologies and electrical conductivity of composite materials, $La_{0.67}Pb_{0.33}MnO_3$, $La_{0.67}Pb_{0.33}CoO_3$ compounds and 90%$La_{0.67}Pb_{0.33}MnO_3$ + 10%A and 90%$La_{0.67}Pb_{0.33}CoO_3$ + 10%A (A= MnO_2, NiO, SnO_2 and Cu_2O), were investigated. As a result of the X-ray diffraction (XRD) analysis, it was found that all samples have trigonal crystal symmetry ($R\bar{3}c$). The refinements have demonstrated that MnO_2, NiO, SnO_2, and Cu_2O compounds, which are employed in the production of composite materials, are present within both the perovskite crystal structure of these compounds and as a secondary phase in the composite materials. The results from AFM and SEM analyses align with those from XRD refinement. Electrical resistivity measurements (ρ-T) were conducted to ascertain the metal-insulator phase transition temperatures (T_{IM}) of various compounds and composite materials. While $La_{0.67}Pb_{0.33}MnO_3$ compound and these compound-based composite materials exhibited a clear T_{IM} phase transition, no T_{IM} phase transition was observed in the $La_{0.67}Pb_{0.33}CoO_3$ compound and these compound-based composite materials.

1. Introduction

Magnetic cooling is based on the utilization of the magnetic phase transformation (paramagnetic-ferromagnetic) that occurs in a magnetic material used as a cooling element during the cooling process. When an external magnetic field is applied to a magnetic material, the magnetic entropy of the material changes as the spins are forced to orient in the direction of the applied field, and the adiabatic temperature change that occurs is known as the "magnetocaloric effect" (MCE). In particular, Gd and some Gd-based (GdSiGe) alloys [1-3] and oxide-containing $La_{1-x}A_xMnO_3$ manganite compounds [4-6] are materials with potential applications in these technologies. Due to their potential to be used as cooling elements in magnetic cooling technologies, manganite compounds have been extensively studied until recently [7-9]. Some of the superior properties of these compounds are that they are easy to produce and the raw materials used in their production are inexpensive, they can be easily shaped and their paramagnetic-ferromagnetic phase transition temperatures (Curie temperature, T_C) change very abruptly even when very low amounts of elements are doped. The huge changes in the resistivity of these compounds to an applied magnetic field (magneto-resistive effect) have opened new doors for the applications of these compounds [10]. The most well-known applications are magnetic sensors used in measuring or detecting the magnetic field in any environment and in storage devices such as hard disks. As a result of monovalent and divalent elements doping to $LaMnO_3$ perovskite manganite compound, which is known to exhibit insulating and antiferromagnetic properties, the compound gains both conductive and ferromagnetic properties. The degree of electrical and magnetic properties depends on the amount and valence of the doped element. Because these properties are highly dependent on the number of Mn^{3+} and Mn^{4+} ions present in the compound. The doping of 1+ valence element in the compound $La^{3+}Mn^{3+}O_3^{2-}$ oxidizes two of the Mn^{3+} ions in the perovskite structure to Mn^{4+}, while the doping of 2+ valence element oxidizes one of the Mn^{3+} ions to Mn^{4+} ions. Initially, the Mn^{3+} ions in the compound $La^{3+}Mn^{3+}O_3^{2-}$ only have Mn^{3+}-O^{2-}-Mn^{3+}

[1]*Department of Physics, Faculty of Science, Muğla Sıtkı Koçman University, 48000, Muğla, Türkiye,* [2]*Department of Chemistry, Faculty of Science, Muğla Sıtkı Koçman University, 48000, Muğla, Türkiye*

#Corresponding author:barisaltan.mu@gmail.com

Keywords: TIM; Magnetic Cooling; Perovskite Magnanites; XRD; SEM; Composites

Received: 07 May 2025 | Accepted: 27 November 2025 | Published online: 30 December 2025

antiferromagnetic interactions (super-exchange), Mn^{3+}-O^{2-}-Mn^{3+}, Mn^{4+}-O^{2-}-Mn^{4+} and Mn^{3+}-O^{2-}-Mn^{4+} interactions occur in $La_{1-x}A_xMnO_3$ manganite compounds obtained as a result of doping. In the first two interactions no free electron movement occurs in the crystal lattice forming the perovskite structure (super-exchange), while in the last interaction, free electron movement (double-exchange) occurs and the material gains both conductivity and ferromagnetic properties. The probability and dominance of these interactions in the materials produced are highly influential on the T_C and MCE values of the materials. Therefore, the focus of the studies on these compounds is to obtain high MCE values under low magnetic field, with T_C values around room temperature, which is important for technological applications. There are several studies on $La_{1-x}A_xMnO_3$ manganite compounds, in which monovalent and divalent elements doping and both of these doping are performed at the same time [11, 12]. In these studies, it has been shown that super-exchange and double-exchange interactions of Mn ions significantly affect both T_C and MCE. Additionally, physical properties such as anisotropy constants, crystal structure symmetries, defects, ionic radius mismatch from elemental doping, selected compound compositions, purity of starting materials, and atomic order lengths in the crystal structure are also effective. Recently, studies on composite materials obtained by combining manganite compounds with different crystal symmetry and different T_C values have intensified [13, 14].

Based on this motivation, in this study, MnO_2, NiO, SnO_2 and Cu_2O compounds were added to $La_{0.67}Pb_{0.33}MnO_3$ and $La_{0.67}Pb_{0.33}CoO_3$ compounds produced by sol-gel method with the help of ultrasonic mixing method to produce $90\%La_{0.67}Pb_{0.33}MnO_3$ + 10%A and $90\%La_{0.67}Pb_{0.33}CoO_3$ + 10%A (A= MnO_2, NiO, SnO_2 and Cu_2O) composite materials produced by ultrasonic vibrator.

2. Results and Discussion

2.1. XRD analysis

2.1.1. XRD Analysis of $90\%La_{0.67}Pb_{0.33}CoO_3$ + 10%A (A= MnO_2, NiO, SnO_2 and Cu_2O) Composite Materials

The XRD refinement program Material Analysis Using Diffraction (MAUD) was used to find the crystal structure symmetries and lattice parameters of the $La_{0.67}Pb_{0.33}CoO_3$ cobaltite compound and four different composite materials. XRD patterns of $La_{0.67}Pb_{0.33}CoO_3$ compound and composite materials obtained after refinement are shown in Figure 1. The crystal structure symmetries, crystal lattice parameters and percent volume phase ratios obtained as a result of the treatment are also given in Table 1. Based on the width of the main peak (2θ=32° to 33°) of the cobaltite compound and composite materials, it is possible to say that they are not fully crystallized. $La_{0.67}Pb_{0.33}CoO_3$ cobaltite compound and four different composite materials were found to have trigonal crystal symmetry with $R\bar{3}c$ space group. In addition to the peaks belonging to the perovskite phase in the composite materials, it is seen that new peaks are formed at different angles depending on the doped oxide compound. As a result of the refinements, it was found that these peaks originate from MnO, NiO, SnO and CuO compounds in the crystal structure as secondary phase. These results showed that the compounds used to form the composite material were located as two separate phases in the composite material and no new compounds were formed despite the heat treatment applied. No significant change was observed in the "*a*" lattice parameter of the perovskite phase in the composite materials obtained as a result of doping NiO, SnO_2 into $La_{0.67}Pb_{0.33}CoO_3$ cobaltite compound, while a partial increase was observed in the "*c*" lattice parameters. However, it was found that significant changes occurred in both "*a*" and "*c*" lattice parameters of the perovskite phase in the composite materials obtained as a result of MnO_2 and Cu_2O doping to $La_{0.67}Pb_{0.33}CoO_3$ cobaltite compound. This is associated with the conclusion that some of the Mn and Cu ions may have replaced Co ions in the center of the octahedral structure in the perovskite phase.

2.1.2. XRD Analysis of $90\%La_{0.67}Pb_{0.33}MnO_3$ + 10%A (A= MnO_2, NiO, SnO_2 and Cu_2O) Composite Materials

XRD patterns of $La_{0.67}Pb_{0.33}MnO_3$ manganite compound and four different composite materials after treatment are shown in Figure 2. The crystal structure symmetries, crystal lattice parameters and percent volume phase ratios obtained as a result of the treatment are also given in Table 1. The $La_{0.67}Pb_{0.33}MnO_3$ manganite compound and composite materials were found to have trigonal crystal symmetry with $R\bar{3}c$ space group like the other compounds and composite materials. It was found that no significant changes occurred in the crystal lattice parameters of the perovskite phase in the $La_{0.67}Pb_{0.33}MnO_3$ manganite compound and composite materials. Except for the addition of MnO_2 to the main compound, the other additives were found to take place as secondary phases in the composite material, except for the perovskite phase. However, no impurity phase was observed in the composite material obtained with the addition of MnO_2. This result shows that all Mn ions are contained in the perovskite phase.

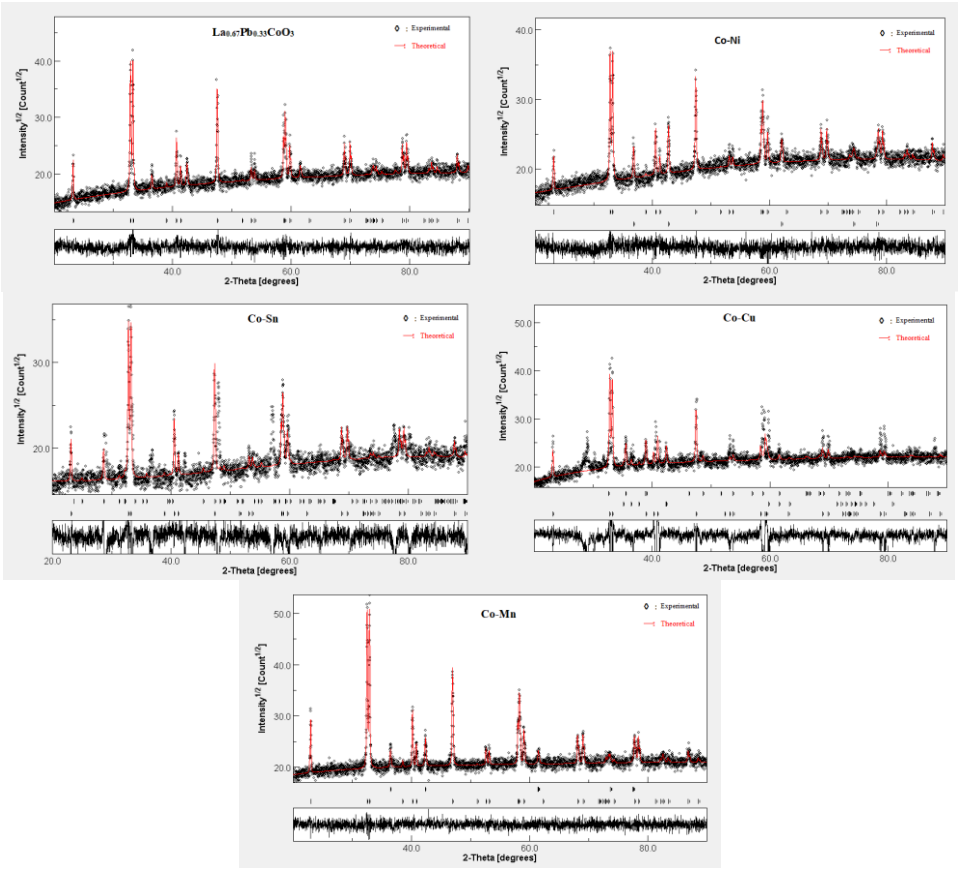

Figure 1. XRD analysis of $La_{0.67}Pb_{0.33}CoO_3$ compound and Co-Ni, Co-Sn, Co-Cu, Co-Mn composite materials.

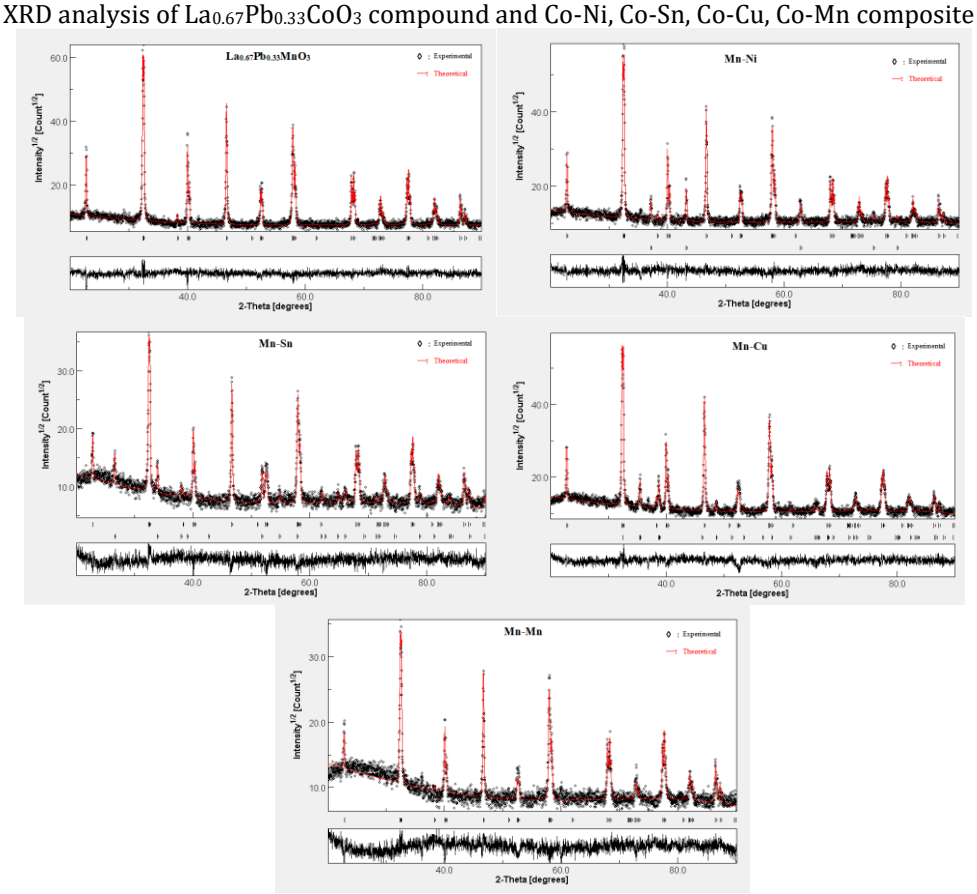

Figure 2. XRD analysis of $La_{0.67}Pb_{0.33}MnO_3$ compound and Mn-Ni, Mn-Sn, Mn-Cu, Mn-Mn composite materials.

Table 1. Crystal structure symmetries, crystal lattice parameters and percent volume phase ratios obtained from XRD refinement.

Compound	Space group	a (Å)	b (Å)	c (Å)	Perovskite phase (%)	Impurity (%)
$La_{0.67}Pb_{0.33}MnO_3$	$R\bar{3}c$	5.5158	5.5158	13.4039	100	-
Mn-Ni	$R\bar{3}c$	5.5125	5.5125	13.3876	93.2	6.8 (NiO)
Mn-Sn	$R\bar{3}c$	5.5197	5.5197	13.4120	93.4	6.6 (SnO)
Mn-Cu	$R\bar{3}c$	5.5185	5.5185	13.3965	94.8	5.2 (CuO)
Mn-Mn	$R\bar{3}c$	5.5174	5.5174	13.4008	100	-
$La_{0.67}Pb_{0.33}CoO_3$	$R\bar{3}c$	5.4416	5.4416	13.0961	100	-
Co-Ni	$R\bar{3}c$	5.4505	5.4505	13.1026	90.8	9.2% (NiO)
Co-Sn	$R\bar{3}c$	54541	5.4541	13.1894	91.2	8.8% (SnO)
Co-Cu	$R\bar{3}c$	5.3797	5.3797	13.4233	92.9	7.1% (CuO)
Co-Mn	$R\bar{3}c$	5.5003	5.5003	13.2413	91.8	8.2%(MnO)

2.2. AFM Analysis

2.2.1. AFM Analysis of 90%$La_{0.67}Pb_{0.33}CoO_3$ + 10%A (A= MnO_2, NiO, SnO_2 and Cu_2O) Composite Materials

AFM images of $La_{0.67}Pb_{0.33}CoO_3$ cobaltite compound and composite materials were taken using contact mode. In the first stage, two-dimensional scanning was performed over the 60 µm × 60 µm area, which is the largest scanning mode of the microscope, and then the studies were completed by gradually reducing the scanning area. In this study, AFM images of $La_{0.67}Pb_{0.33}CoO_3$ compound and composite materials in the 10 µm x 10 µm scanning area are presented. Two- and three-dimensional AFM images of $La_{0.67}Pb_{0.33}CoO_3$ and composite materials are given in Figure 3. From the AFM images of the $La_{0.67}Pb_{0.33}CoO_3$ compound, it is seen that the grains containing plate-like structure are randomly oriented on the surface and there are gaps between the grains. However, it is noticeable that the grain formations on the surface of the composite materials are different from the $La_{0.67}Pb_{0.33}CoO_3$ compound. Especially in the surface formations where large and small grains are intertwined, it is seen that large grains are located higher, and smaller grains are located at the grain boundaries connecting these grains. It is also evident that the intergranular voids seen in the $La_{0.67}Pb_{0.33}CoO_3$ compound are not formed on the surface of the composite materials. It was found as a result of XRD studies that all composite materials consisted of two phases. Therefore, it is possible to say that MnO, NiO, SnO and CuO impurities are located at the grain boundaries connecting the coarse grains. As a result, it is expected that the surface morphologies of the composite compounds are different from $La_{0.67}Pb_{0.33}CoO_3$ and these changes will cause changes in the electrical conductivity behavior of the composite materials.

2.2.2. AFM Analysis of 90%$La_{0.67}Pb_{0.33}MnO_3$ + 10%A (A= MnO_2, NiO, SnO_2 and Cu_2O) Composite Materials

Figure 4 shows two- and three-dimensional AFM images of $La_{0.67}Pb_{0.33}MnO_3$ compound and Mn-Ni, Mn-Sn, Mn-Cu, Mn-Mn composite materials. On the surface of the $La_{0.67}Pb_{0.33}MnO_3$ compound, well crystallized grains of different sizes are seen to be tightly packed together. It can be clearly said that the grains on the surface of the compound are formed by the arrangement of overlapping layers in different directions (this can be seen more clearly in the three-dimensional image of the compound). Except for Mn-Mn and Mn-Ni, the surface morphology of the other composite materials is clearly different. In the Mn-Sn composite material, small grain clusters are seen surrounding the coarse grains on the surface. These small grain clusters are thought to be the SnO secondary phase revealed in XRD studies. On the surface of the Mn-Cu composite material, serrated and ordered large grain formations stand out. Next to the serrated grains, other spherical grain formations are also noticeable (see three-dimensional image). These two different grain formations coincide with the two different phases obtained in XRD studies.

2.3. SEM Studies

2.3.1. SEM Studies of 90%$La_{0.67}Pb_{0.33}CoO_3$ + 10%A (A= MnO_2, NiO, SnO_2 and Cu_2O) Composite Materials

Figure 5 shows the SEM images of $La_{0.67}Pb_{0.33}CoO_3$ compound and Co-Ni, Co-Sn, Co-Cu, Co-Mn composite materials obtained at 3000 magnification. It is seen that the surface morphology of the $La_{0.67}Pb_{0.33}CoO_3$ compound consists of grains of different shapes, sizes and geometries. These grains grow on each other in different directions. Plate-like formations on the surface of the compound and the presence of very small grains between and above the grains/plates are noticeable. It is seen that the surface of this composite does not consist of tightly packed grains and a homogeneous structure. However, the surface structuring of the composite materials in general was quite different from the surface of the

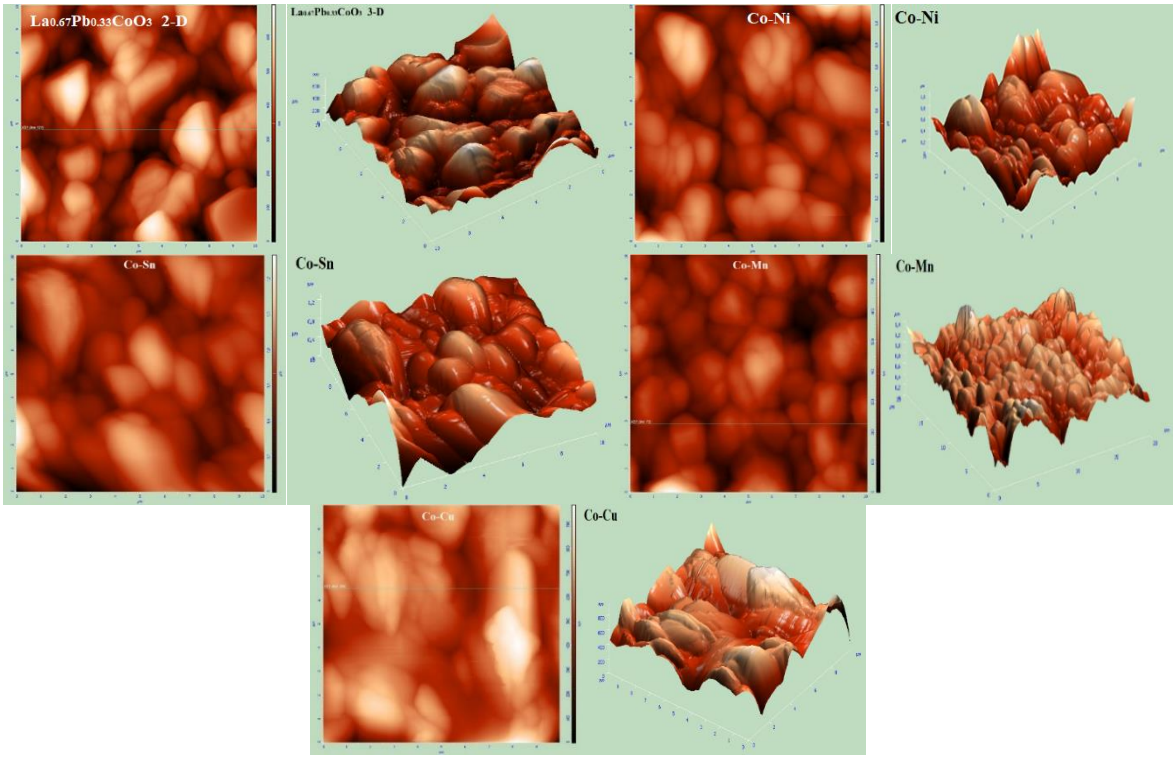

Figure 3. Two- and three-dimensional AFM images of $La_{0.67}Pb_{0.33}CoO_3$ compound and Co-Ni, Co-Sn, Co-Cu, Co-Mn composite materials.

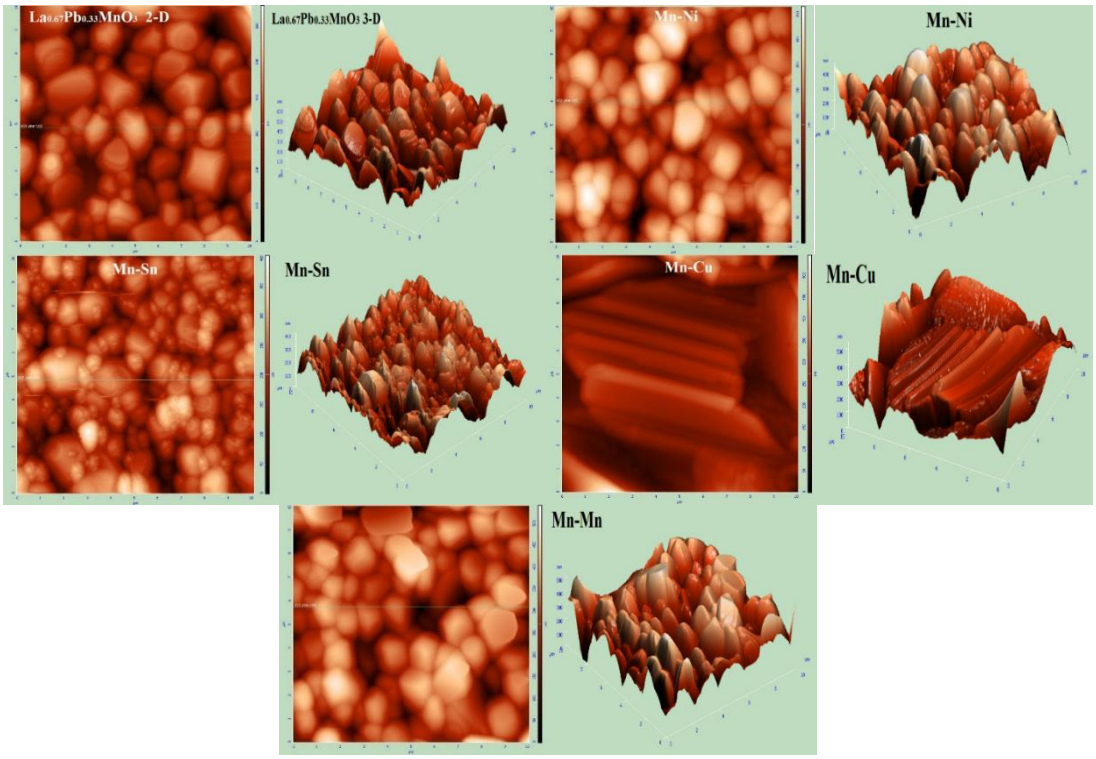

Figure 4. Two- and three-dimensional AFM images of $La_{0.67}Pb_{0.33}MnO_3$ compound and Mn-Ni, Mn-Sn, Mn-Cu, Mn-Mn composite materials.

$La_{0.67}Pb_{0.33}CoO_3$ compound. On the surfaces of these materials (except Co-Cu), two separate grain groups differing in size from each other are observed. These coarse and small grains are packed together tightly, and in general, the surface grains are much smaller than those found on the surface of the

$La_{0.67}Pb_{0.33}CoO_3$ compound. It was found that the small grains on the surface of the composite materials are more dominant (perovskite phase), while the larger grains from the EDS studies belong to the secondary phases, as revealed by XRD analysis. The surface morphology of the Co-Cu composite material appears to be different from other composite materials. The formation of different structures cannot be directly distinguished on the surface of this material. A thin plate-like structure (similar to the $La_{0.67}Pb_{0.33}CoO_3$ compound) with random orientation has formed on the surface of this material.

2.3.2. SEM Studies of 90%$La_{0.67}Pb_{0.33}MnO_3$+ 10%A (A= MnO_2, NiO, SnO_2 and Cu_2O) Composite Materials

Figure 6 shows the SEM images of $La_{0.67}Pb_{0.33}MnO_3$ compound and Mn-Ni, Mn-Sn, Mn-Cu, Mn-Mn composite materials obtained at 3000 magnification. On the surface of the $La_{0.67}Pb_{0.33}MnO_3$ compound, the formation of a surface that is almost void-free and where grains ranging in size from 1-3 μm form a tightly packed structure is noticeable. A void-free structure is also observed on the surface of the composite materials. Except for Mn-Mn and Mn-Ni composite materials, two different structures clearly appear on the surfaces of composite materials. The different structure on the surface of Mn-Sn and Mn-Co composite materials is thought to be due to two different compounds, which were also obtained in XRD analysis. It is seen that the surfaces of Mn-Mn and Mn-Ni composite materials resemble the surface of $La_{0.67}Pb_{0.33}MnO_3$ compound in terms of formation, except for grain size. Based on the fact that no secondary phase was found in the XRD analysis of Mn-Mn and Mn-Ni composite materials and the surface formations, it is possible to say that both Mn and Ni ions are involved in the perovskite structure.

2.4. R-T Measurements

2.4.1. R-T Measurements of 90%$La_{0.67}Pb_{0.33}CoO_3$ + 10%A (A= MnO_2, NiO, SnO_2 and Cu_2O) Composite Materials

In order to determine the temperature dependent resistivity behavior of $La_{0.67}Pb_{0.33}CoO_3$ compound and composite materials and possible metal-insulator phase transition temperatures (T_{IM}), electrical resistivity measurements were performed using the four-contact method. In the ρ-T curve of $La_{0.67}Pb_{0.33}CoO_3$ compound and composite materials given in Figure 7, it is seen that there is a very slow increase in resistance values starting from high temperatures and decreasing towards low temperature regions. This is an indication of a transition from a semi-metallic behavior or semiconductor state to an insulator state depending on the decrease in temperature for all compounds. However, in $La_{0.67}Pb_{0.33}CoO_3$ compound and composite materials, a very sudden increase in resistance values was observed after a certain temperature value. The temperature at which such a sudden increase in resistance begins is known as the charge-ordering (CO) temperature. CO is a mechanism observed in perovskite compounds containing mixed valence elements and has attracted much attention in recent years [15, 16] and is a (first or second order) phase transition that occurs mostly in materials such as metal oxides or organic conductors. The temperature-dependent CO phase leads to very abrupt changes in the electric and magnetic properties due to the localization of charges in different regions leading to disproportionality and an ordered superlattice, due to complex interactions between spin, orbital and lattice degrees of freedom [17]. In Figure 7, the value of CO phase transition temperatures of $La_{0.67}Pb_{0.33}CoO_3$ compound and composite materials were determined by means of the plots of $d(ln(\rho/T))$ plotted against T, which is shown as an inner-graph in ρ-T plots. The CO phase transition temperature of $La_{0.67}Pb_{0.33}CoO_3$ was calculated as 218.4 K and it was found that the CO transition temperatures of the other composites, except the Co-Cu composite material, were lower than that of $La_{0.67}Pb_{0.33}CoO_3$. It is known that the inhomogeneous distribution of the main phase and secondary phases in materials containing two different phases, such as these composite materials, is highly effective on the conductivity properties of the materials [18]. In the SEM study, which revealed that $La_{0.67}Pb_{0.33}CoO_3$ based composite materials consisted of two different phases, it was determined that the large grains on the surfaces of these materials belonged to secondary phases such as NiO, MnO, and SnO. The secondary phases in the structure act as irregular clusters of defects, which have a significant blocking effect on the movement paths of free electrons and are therefore known to lead to an increase in the electrical resistivity of the materials. In composite materials such as Co-Ni and Co-Mn, insulating secondary phases like NiO and MnO (identified in XRD analyses [19, 20]) are present. It is thought that these phases inhibit the free movement of electrons and/or act as defect spots that trap free electrons. By acting as such barriers, they consequently cause

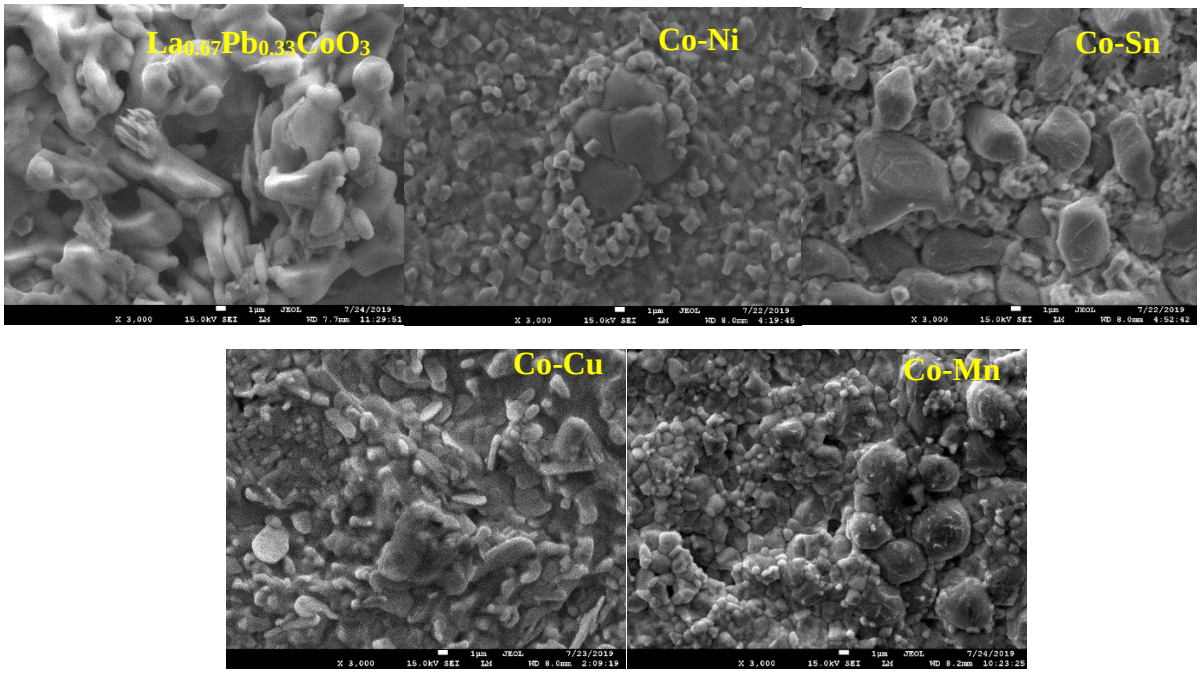

Figure 5. SEM images of $La_{0.67}Pb_{0.33}CoO_3$ compound and Co-Ni, Co-Sn, Co-Cu, Co-Mn composite materials.

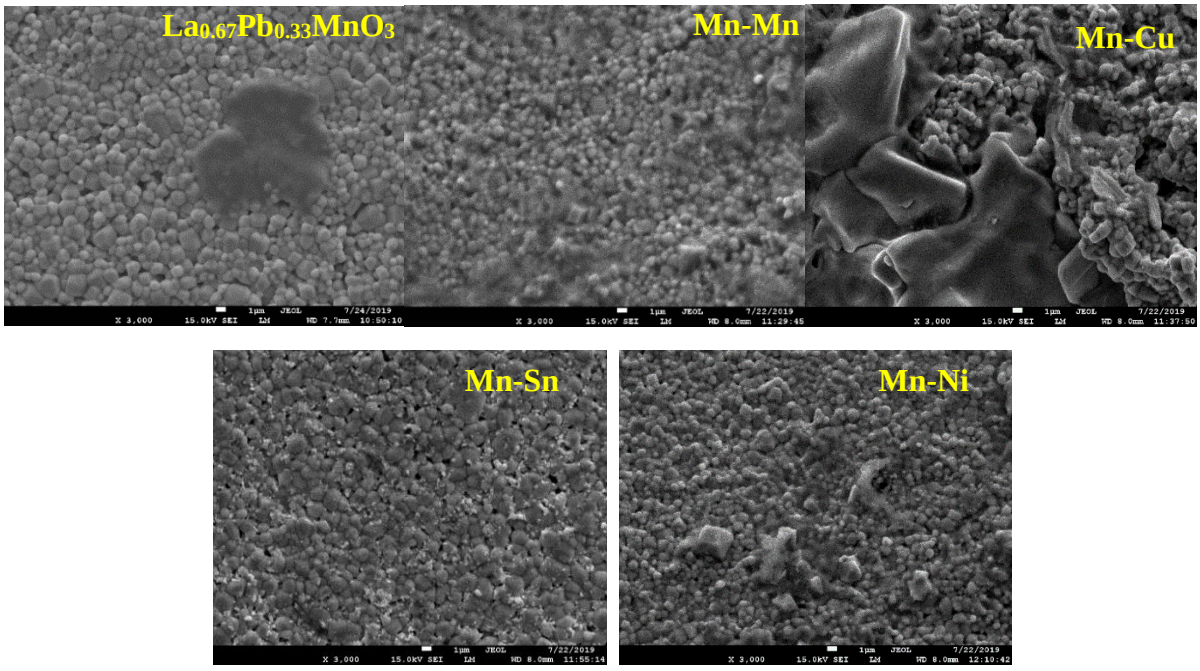

Figure 6. SEM images of $La_{0.67}Pb_{0.33}MnO_3$ compound and Mn-Ni, Mn-Sn, Mn-Cu, Mn-Mn composite materials.

the CO phase in these composites to occur below the transition temperature of the CO phase in the $La_{0.67}Pb_{0.33}CoO_3$ compound. Because the grain sizes of the primary and secondary phases are very different and due to their inhomogeneous distribution in the materials, pores and/or voids are likely to occur at the grain boundaries. Such pore and void formations are not desirable and are known to have a negative effect on electrical resistance by limiting the mobility of electrons moving freely within the materials [18]. Among the composite materials, only the CO phase transition temperature of the Co-Cu composite material was found to be higher than the CO phase transition temperature of the $La_{0.67}Pb_{0.33}CoO_3$ composite (275.2 K). This result shows that the Co-Cu composite material has the best electrical properties in this series. In the XRD analysis, the Co-Cu composite material was found to have the lowest secondary phase ratio among the composite

materials. This was explained as being due to the presence of some Cu ions in the perovskite structure. Because it is known from the literature that the ionic radius of Cu^{3+} ion (0.540 Å) and the ionic radius of Co^{3+} ion (0.545 Å) are almost the same [21]. Therefore, we can say that during the heat treatment process applied to the Co-Cu composite material, some Cu ions pass into the perovskite structure by settling in the center of the octahedral where Co ions are located. Thus, it can be said that Cu^{+3} ions in the center of some octahedral, by ferromagnetic interaction with Co ions in the center of adjacent octahedral through oxygen ions [22, 23], improve the electrical properties of the composite material.

2.4.2. R-T Measurements of 90%$La_{0.67}Pb_{0.33}MnO_3$ + 10%A (A= MnO_2, NiO, SnO_2 and Cu_2O) Composite Materials

Figure 8 shows the ρ-T curves of $La_{0.67}Pb_{0.33}MnO_3$ compound and Mn-Ni, Mn-Sn, Mn-Cu and Mn-Mn composite materials. In manganite compounds, the resistivity generally increases with decreasing temperature ($d\rho/dT$<0) and reaches a maximum value. The temperature ($d\rho/dT$= 0) at which the peak (maximum value) appears in the ρ-T curve is known as the metal-insulator (metal-semiconductor) phase transition temperature (T_{IM}) of the materials. In the temperature region below this value ($d\rho/dT$>0), compounds exhibit metallic material behavior due to their conductive properties [24]. From Figure 8 it is clear from the graphs that all materials have a T_{IM} peak. The T_{IM} transition temperatures of $La_{0.67}Pb_{0.33}MnO_3$ compound and Mn-Ni, Mn-Sn, Mn-Cu and Mn-Mn composite materials were found to be 262.4 K, 264.4 K, 270.4 K, 286.6 K and 299.2 K, respectively. As can be clearly seen from the values, the T_{IM} transition temperatures of the composite materials were higher than those of $La_{0.67}Pb_{0.33}MnO_3$. In the XRD pattern analysis of $La_{0.67}Pb_{0.33}MnO_3$ compound and Mn-Ni, Mn-Sn, Mn-Cu and Mn-Mn composite materials, it was found that some NiO, $SnO_2$and Cu_2O entered the perovskite structure and a certain amount of CuO, SnO and NiO as secondary phases were found in the composite material. SEM analysis also revealed that the grains of the secondary phases were smaller than the grains of the perovskite phase in the composite material. It is seen that the low proportion of secondary phases in the composite materials and the very small grain sizes do not have a negative effect on the T_{IM} phase transition temperature of the materials. The higher T_{IM} values of the composite materials compared to the $La_{0.67}Pb_{0.33}MnO_3$ compound are attributed to the presence of Cu, Sn, Mn, and Ni ions, which, as revealed by XRD analysis, partially integrate into the perovskite structure. Therefore, it will be possible to explain these situations based on the possible states of the valences of the ions entering the perovskite structure.

The T_{IM} phase transition temperature of the Mn-Ni composite material was found to occur 2 K higher than the $La_{0.67}Pb_{0.33}MnO_3$ compound. If the Ni ions entering the perovskite structure are 3+ valence, Ni^{3+}-O^{2-}-Mn^{3+} interactions will occur in the perovskite structure and these interactions will cause a spontaneous magnetization in the compound [25]. If Ni ions enter the perovskite structure with 2+ valence, then Ni^{4+}-O^{2-}—Mn^{2+} ferromagnetic interactions will occur, and the probability of this interaction is more stable and higher than Ni^{3+}-O^{2-}-Mn^{3+} interactions [26]. As a result, it can be concluded that ferromagnetic behavior (conductivity) will increase in both interactions. The slight increase in the T_{IM} phase transition temperature of the Mn-Ni composite material suggests that some Ni ions are incorporated into the perovskite structure.

The T_{IM} phase transition temperature of the Mn-Sn composite material was calculated as 270.4 K. It is known from the literature that the substitution of Sn ions for Mn at the octahedral does not affect ferromagnetism but lowers the Curie temperatures due to the possibility of Sn^{4+}-O^{2-}-Mn^{4+} and Sn^{4+}-O^{2-}-Sn^{4+} super-exchange interactions [27]. The degree of ferromagnetic behavior occurring in manganite compounds does not only depend on the interactions between Mn ions. It is also necessary to consider the changes in bond lengths and bond angles in the octahedral in the perovskite structure. The Sn ions considered to be in the perovskite structure have only 4+ valence and the ionic radius of Sn^{4+} (0.69 Å) is larger than the ionic radius of both Mn^{3+} (0.645 Å) and Mn^{4+} (0.53 Å). Therefore, as a result of Sn^{4+}-O^{2-}-Mn^{4+} and Sn^{4+}-O^{2-}-Sn^{4+} interactions that are likely to exist within the perovskite structure, changes will occur in the bond angles and bond lengths in the octahedral in certain regions within the perovskite structure. In some cases, such changes and distortions are known to contribute to the facilitation of the movement paths of free-moving electrons in the crystal structure, leading to increased conductivity [28]. Therefore, it is thought that the increase in the T_{IM} phase transition temperature of the Mn-Sn composite material is due to the change in the bond angle and

NANOSAM
Journal of NanoScience in Advanced Materials

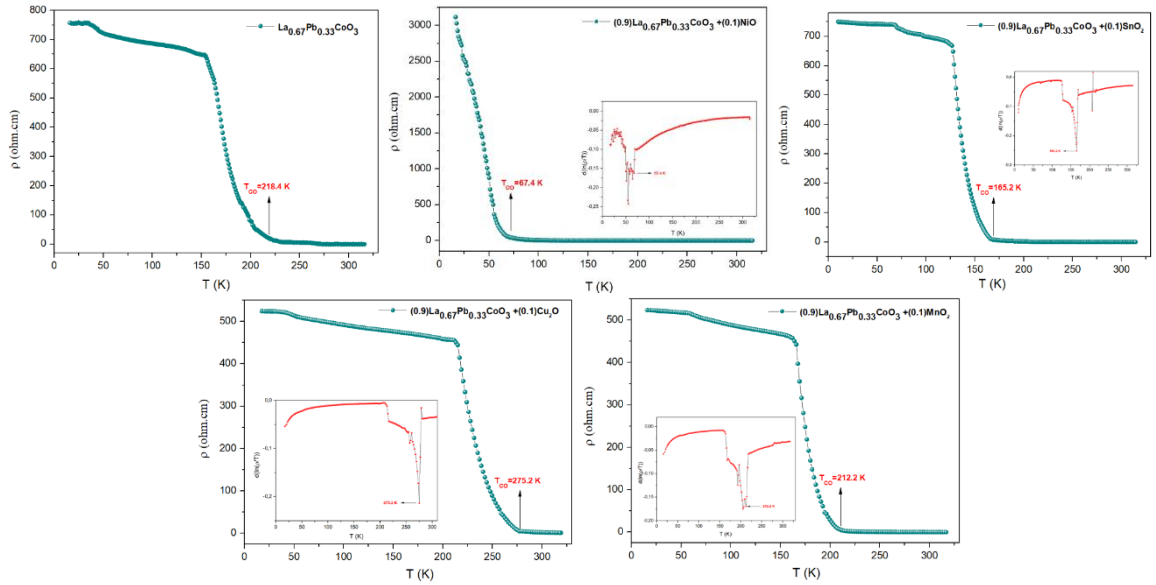

Figure 7. R-T measurements of 90%$La_{0.67}Pb_{0.33}CoO_3$ + 10%A (A= MnO_2, NiO, SnO_2 and Cu_2O) composite materials.

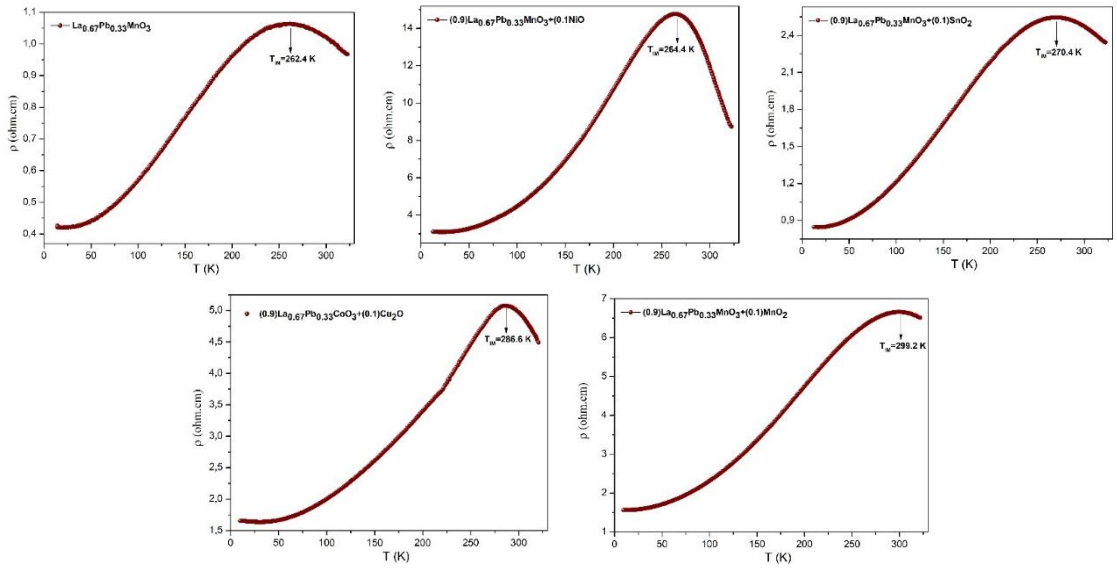

Figure 8. ρ-T curves of $La_{0.67}Pb_{0.33}MnO_3$ compound and Mn-Ni, Mn-Sn, Mn-Cu and Mn-Mn composite materials.

bond lengths at the octahedral due to the radius mismatch as a result of some Sn ions entering the perovskite structure.

The T_{IM} phase transition temperature of the Mn-Cu composite material was found to occur at 270.4 K, 24.2 K higher than that of the $La_{0.67}Pb_{0.33}MnO_3$ composite. Two different scenarios can be mentioned to explain the increasing T_{IM} phase transition temperature for the Mn-Cu composite material. The first is the valence of Cu ions in the perovskite structure and the second is the possible changes in the Mn/Cu-O bond length and Mn/Cu-O-Mn/Cu bond angles according to the number of Cu ions in the perovskite structure. As a result of Cu doping in perovskite manganite compounds, studies on the valence of Cu ions in the crystal structure are available in the literature [29, 30]. The results obtained in these studies reveal that Cu ions are together in the crystal structure as a mixed state of 2+ and 3+, with Cu^{2+} being dominant. The coexistence of Cu^{2+} and Cu^{3+} ions in Mn-Cu composite material with Cu^{2+} dominance changes the Cu^{2+}/Cu^{3+} ratio and therefore the Mn^{3+}/Mn^{4+} ratio. In this case, the crystal structure and lattice parameters are affected due to the ionic radius mismatch between Cu and Mn ions. The ionic radius of Cu^{2+} (0.73 Å) is larger than the ionic radii of Mn^{3+} and Mn^{4+} in the B-site, while the ionic radius of Cu^{3+} (0.54 Å) is smaller than the ionic radius of Mn^{3+} (0.645 Å) and very close to the ionic radius of Mn^{4+}

(0.53 Å). Therefore, Cu^{2+} ions are expected to replace Mn^{3+} ions and Cu^{3+} ions are expected to replace Mn^{4+} ions in the crystal structure [31]. Depending on the replacement of Mn^{3+} ions by Cu^{2+} and Mn^{4+} by Cu^{3+} ions in the octahedral in the perovskite structure, there will be a gradual transformation of Mn^{3+} to Mn^{4+} and/or Mn^{4+} to Mn^{3+} in the perovskite structure. In the Mn-Cu composite material, the number of Mn^{3+} ions will decrease as a result of Cu ions entering the perovskite structure with a more dominant 2+ valence, while the number of Mn^{4+} ions, which is theoretically 33% in the $La_{0.67}Pb_{0.33}MnO_3$ compound, will increase. Due to this increase, the charge carriers involved in the pairwise exchange interactions between Mn^{3+} and Mn^{4+}, which show conductive and ferromagnetic properties, will find the opportunity to pass more easily depending on the changing conditions (transition distance and energy) and will contribute positively to the conductivity [32]. For the Mn-Cu composite material, the ρ-T curve suggests that the charge ordering (CO) phase occurs at a higher temperature than in the pure $La_{0.67}Pb_{0.33}MnO_3$compound. This shift is attributed to the presence of mixed valences (Cu^{2+}/Cu^{3+} and Mn^{3+}/Mn^{4+}) at the Mn sites within the perovskite octahedra. The changing pairwise exchange interactions from these mixed valences lead to alterations in the Mn/Cu-O bond lengths and Mn/Cu-O-Mn/Cu bond angles, which consequently affect the CO transition temperature. The T_{IM} phase transition temperature of the Mn-Mn composite material was found to be approximately 299.2 K, which is very close to room temperature. This value is 36.8 K higher than the T_{IM} phase transition temperature of the $La_{0.67}Pb_{0.33}MnO_3$ composite. In fact, $La_{0.67}Pb_{0.33}MnO_3$ compound and Mn-Mn composite material seem to be the same compounds, but they have differences in terms of the valence states of the Mn ions they contain. Theoretically, 33% of the Mn ions in the $La_{0.67}Pb_{0.33}MnO_3$ compound have 4+ valence. Therefore, there is a 33% (theoretical maximum) probability of a Mn^{3+}-O^{2-}-Mn^{4+} double exchange interaction occurring, which would give this compound conductivity and ferromagnetic properties. However, it is also possible for Mn^{4+} ions to have Mn^{4+}-O^{2-}-Mn^{4+} super-exchange interactions among themselves, which are antiferromagnetic. In summary, it is unlikely (low probability) that all Mn^{4+} ions in this compound will have double exchange interactions. In the Mn-Mn composite material obtained in the study, it was revealed in XRD and SEM studies that Mn ions in MnO_2 entered the structure of $La_{0.67}Pb_{0.33}MnO_3$ perovskite manganite compound. The Mn ions in the MnO_2 compound used to form the Mn-Mn composite material are 4+ valence and as a result of the entry of these ions into the perovskite structure, the number of Mn^{4+} ions in the perovskite structure increased. Due to this increase, the probability of Mn^{3+}-O^{2-}-Mn^{4+} double exchange interaction also increased and the T_{IM} phase transition of the Mn-Mn composite material occurred at higher temperatures than that of the $La_{0.67}Pb_{0.33}MnO_3$ perovskite manganite compound.

3. Conclusion

This study successfully synthesized and characterized composite materials based on $La_{0.67}Pb_{0.33}MnO_3$ and $La_{0.67}Pb_{0.33}CoO_3$ perovskites with 10% additions of MnO_2, NiO, SnO_2, and Cu_2O.

XRD refinements confirmed the incorporation of dopant ions into the perovskite structures, with a higher degree of integration observed in the $La_{0.67}Pb_{0.33}MnO_3$-based composite materials. This incorporation induced significant changes in the crystal lattice parameters, attributable to the ionic radius differences of the substituted cations. SEM and AFM analyses corroborated the presence of secondary phases, which were distributed as clusters within the composites.

Electrical transport measurements revealed distinct behaviors. In $La_{0.67}Pb_{0.33}CoO_3$-based composite materials, the metal-insulator transition (T_{IM}) was suppressed, replaced by a semiconductor-to-insulator transition and a shift of the charge ordering (CO) temperature to lower values. This is attributed to the disruptive influence of secondary phases on the conduction mechanism. In contrast, all $La_{0.67}Pb_{0.33}MnO_3$-based composite materials exhibited a T_{IM} transition, with transition temperatures higher than that of the parent $La_{0.67}Pb_{0.33}MnO_3$ compound (262.4 K). The increase in T_{IM} temperature was directly correlated with the volume fraction of dopant ions integrated into the perovskite structure, as determined by XRD.

The principal achievement of this work is the demonstration that compositing is an effective strategy for tuning phase transition temperatures. Specifically, we have shown that the T_{IM} transition of $La_{0.67}Pb_{0.33}MnO_3$-based composite materials can be systematically optimized toward room temperature, a critical requirement for advancing their application in solid-state cooling technologies.

Method

$La_{0.67}Pb_{0.33}MnO_3$ and $La_{0.67}Pb_{0.33}CoO_3$ perovskite manganite compounds used as the main material in the study were produced using the sol-gel method. Detailed information about the beginning of the sol-gel method, production steps, citric acid-ethyl alcohol amounts used for chelating and heating steps in the magnetic stirrer can be found in

reference [28]. In order to combine $La_{0.67}Pb_{0.33}MnO_3$ and $La_{0.67}Pb_{0.33}CoO_3$ manganite compounds and MnO_2, NiO, SnO_2, and Cu_2O_3 oxide compounds obtained in nano size by burning at 600 ° C as composite materials, ultrasonic bath method was used as a mixing technique. In this step, eight different composite powder materials with the compositions $90\%La_{0.67}Pb_{0.33}MnO_3$ + 10%A and $90\%La_{0.67}Pb_{0.33}CoO_3$ + 10%A (A= MnO_2, NiO, SnO_2 and Cu_2O) were prepared by weighing. These powders were then dissolved in alcohol, mixed for one hour using an ultrasonic bath stirring technique to ensure homogeneity, and finally left to dry in an oven. After this stage, one gram each of the $La_{0.67}Pb_{0.33}MnO_3$ and $La_{0.67}Pb_{0.33}CoO_3$ parent compounds and eight composite materials were compacted into circular tablets (diameter of 1.3 cm) using a hydraulic press under a load of 3-4 tons. In the final step, the tablets were sintered in an adjustable high temperature furnace at 1000 °C for 24 hours in air to crystallize the parent compounds and composite materials. For easier understanding of the samples, the manganite composite materials of $90\%La_{0.67}Pb_{0.33}MnO_3$ + 10%A (A= MnO_2, NiO, $SnO_2$and Cu_2O) were analyzed as Mn-Mn, Mn-Ni, Mn-Sn and Mn-Cu, respectively, and $90\%La_{0.67}Pb_{0.33}CoO_3$ + 10%A (A= MnO_2, NiO, SnO_2 and Cu_2O) composite materials will be abbreviated as Co-Mn, Co-Ni, Co-Sn and Co-Cu.

Bruker D8 Advance X-ray diffractometer (XRD) was used to find the crystal symmetries and lattice parameters of the parent compound and composite materials and measurements were made between $20^o<2\theta<90^o$ in $0{,}01^o$ steps. Atomic force microscopy (AFM) and field emission scanning electron microscopy (FE-SEM) with energy dispersive x-ray spectroscopy (EDS) (JEOL, JSM 5800) were used to determine the grain formations on the surface of the compounds (grain bonding, voids, etc.) and to calculate the grain sizes. In order to find the metal-insulator (T_{IM}) phase transition temperatures of the compounds, temperature-varying resistance (ρ-T) measurements were performed. The measurements were carried out on sintered pellets using a standard four-probe configuration with silver paste and attached copper wires to ensure good ohmic contact. The data were collected using a Janis low-temperature closed-circuit cryostat system operating in the temperature range of 10-320 K.

Acknowledgement

This work was performed at The Research and Application Centre For Research Laboratories, Muğla Sıtkı Koçman University. The authors express their gratitude to Prof. Dr. Atilla Coşkun for providing laboratory facilities and guidance.

Authors' Contributions

BA: Performing and conducting experiments/data collection, data analysis and interpretation, drafted the paper. **ECÖ:** Sample preparation and experiments. **ENB:** Sample preparation and experiments.

Data Availability Statement

The data that support the findings of this study are available from the corresponding author upon reasonable request.

Declaration of Ethical Standards

The author(s) of this article declare that the materials and methods used in this study do not require ethical committee permission and/or legal-special permission.

Conflict of Interest

There is no conflict of interest in this study.

References

[1] Pecharsky, V.K., Gschneidner, J., K A, Giant Magnetocaloric Effect in $Gd_5(Si_2Ge_2)$, Physical Review Letters **78**, 4494-4497 (1997).

[2] Pecharsky, V.K., Gschneidner, K.A., Phase relationships and crystallography in the pseudobinary system Gd_5Si_4-Gd_5Ge_4, Journal of Alloys and Compounds **260** (1), 98-106 (1997).

[3] Gschneidner, K.A., Pecharsky, V.K., Magnetocaloric Materials, Annual Review of Materials Research **30**, 387-429 (2000).

[4] Nguyen, H., Nguyen, T., Preparation and magneto-caloric effect of $La_{1-x}Ag_xMnO_3$ (x= 0.10-0.30) perovskite compounds, Physica B: Condensed Matter **319,** 168-173 (2002).

[5] Guo, Z.B., Du, Y.W., Zhu, J.S., Huang, H., Ding, W.P., Feng, D., Large Magnetic Entropy Change in Perovskite-Type Manganese Oxides, Physical Review Letters **78** (6), 1142-1145 (1997).

[6] Ayaş, A., Akyol, M., Ekicibil, A., Structural and magnetic properties with large reversible magnetocaloric effect in $(La_{1-x}Pr_x)_{0.85}Ag_{0.15}MnO_3$ ($0.0 \leq x \leq 0.5$) compounds, Philosophical Magazine **96,** 1-16 (2016).

[7] Ulyanov, A., Kim, J., Shin, G., Kang, Y., Yoo, S., Giant magnetic entropy change in $La_{0.7}Ca_{0.3}MnO_3$ in low magnetic field, Journal of Physics D: Applied Physics **40,** 123 (2006).

[8] Tian, S.-B., Phan, M.-H., Yu, S.-C., Hur, N.H., Magnetocaloric effect in a $La_{0.7}Ca_{0.3}MnO_3$ single crystal, Physica B: Condensed Matter **327** (2), 221-224 (2003).

[9] Khlifi, M., Dhahri, E., Magnetic, magnetocaloric, magnetotransport and magnetoresistance properties of calcium deficient manganites $La_{0.8}Ca_{0.2-x}\square_xMnO_3$ post-annealed at 800 °C, Journal of Alloys and Compounds **587,** 771 (2014).

[10] Yang, S.a., Chen, Q., Yang, Y., Gao, Y., Xu, R., Zhang, H., Ma, J., Silver addition in polycrystalline $La_{0.7}Ca_{0.3}MnO_3$: Large

magnetoresistance and anisotropic magnetoresistance for manganite sensors, Journal of Alloys and Compounds **882,** 160719 (2021).

[11] Kalyana Lakshmi, Y., Venkataiah, G., Vithal, M., Venugopal Reddy, P., Magnetic and electrical behavior of $La_{1-x}A_xMnO_3$ (A=Li, Na, K and Rb) manganites, Physica B: Condensed Matter **403** (18), 3059-3066 (2008).

[12] Hsini, M., Ghivelder, L., Parisi, F., Critical behavior investigated through magnetocaloric effect in PrSrMnO and Pr(Sr,Ca)MnO manganites, Journal of Magnetism and Magnetic Materials **535,** 168059 (2021).

[13] Pękała, M., Pękała, K., Drozd, V., Fagnard, J.F., Vanderbemden, P., Effect of nanocrystalline structure on magnetocaloric effect in manganite composites $(1/3)La_{0.7}Ca_{0.3}MnO_3/(2/3)La_{0.8}Sr_{0.2}MnO_3$, Journal of Alloys and Compounds **629,** 98-104 (2015).

[14] Wang, G.F., Zhao, Z.R., Li, H.L., Zhang, X.F., Enhancement of refrigeration capacity and table-like magnetocaloric effect in $La_{0.8}Ca_{0.2}MnO_3/La_{0.8}K_{0.2}MnO_3$ nanocrystalline composite, Ceramics International **41** (7), 9035-9040 (2015).

[15] Daughton, J., Brown, J., Chen, E., Beech, R., Pohm, A., Kude, W., Magnetic field sensors using GMR multilayer, Magnetics, IEEE Transactions on **30,** 4608-4610 (1994).

[16] Chatterji, T., McIntyre, G.J., Caliebe, W., Suryanarayanan, R., Dhalenne, G., Revcolevschi, A., Reentrant behavior of the charge and orbital ordering and antiferromagnetism in $LaSr_2Mn_2O_7$, Physical Review B **61** (1), 570-574 (2000).

[17] Allieta, M., Scavini, M., Lo Presti, L., Coduri, M., Loconte, L., Cappelli, S., Oliva, C., Ghigna, P., Pattison, P., Scagnoli, V., Charge ordering transition in $GdBaCo_2O_5$: Evidence of reentrant behavior, Physical Review B **88,** 214104 (2013).

[18] Diez, J.-C., Rasekh, S., Madre, M.A., Torres, M.A., Sotelo, A.E., High thermoelectric performances of Bi–AE–Co–O compounds directionally growth from the melt, Boletín de la Sociedad Española de Cerámica y Vidrio **57** (1), 1-8 (2018).

[19] Bhide, V.G., Dani, R.H., Electrical conductivity in oxides of manganese and related compounds, Physica **27** (9), 821-826 (1961).

[20] Steirer, K.X., Chesin, J.P., Widjonarko, N.E., Berry, J.J., Miedaner, A., Ginley, D.S., Olson, D.C., Solution deposited NiO thin-films as hole transport layers in organic photovoltaics, Organic Electronics **11** (8), 1414-1418 (2010).

[21] Shannon, R., Revised Effective Ionic Radii and Systematic Studies of Interatomic Distances in Halides and Chalcogenides, Acta Cryst **32,** 751-767 (1976).

[22] Ruiz-Díaz, P., Stepanyuk, O., Stepanyuk, V., Effects of exchange interactions on magnetic anisotropy and spin-dynamics of adatoms on metallic surfaces, The Journal of Physical Chemistry C 119 (46), 26237-26241 (2015).

[23] Brovko, O.O., Ignatiev, P.A., Stepanyuk, V.S., Bruno, P., Tailoring Exchange Interactions in Engineered Nanostructures: An Ab Initio Study, Physical Review Letters **101** (3), 036809 (2008).

[24] Coşkun, A., Taşarkuyu, E., Irmak, A.E., Aktürk, S., High magnetic entropy change in $La_{0.70}Ca_{0.21}Ag_{0.09}MnO_3$ compound, Journal of Alloys and Compounds **669**, 217-223 (2016).

[25] Toulemonde, O., Studer, F., Raveau, B., Magnetic interactions studies of Co and Ni-doped manganites using soft XMCD, Solid State Communications **118** (2), 107-112 (2001).

[26] Blasse, G., Ferromagnetic interactions in non-metallic perovskites, Journal of Physics and Chemistry of Solids **26** (12), 1969-1971 (1965).

[27] Jemai, D., Mnefgui, S., Ben Hassine, A., Tahri, T., Oumezzine, M., Behavior of the magnetocaloric effect in $La_{0.7}Ba_{0.2}Ca_{0.1}Mn_{1-x}Sn_xO_3$ manganite oxides as promising candidates for magnetic refrigeration, Physica B: Condensed Matter **537**, 93-97 (2018).

[28] Samancıoğlu, Y., Coşkun, A., Magnetic properties of A- and B-site cation doped $La_{0.65}Ca_{0.35}MnO_3$ manganites, Journal of Alloys and Compounds **507** (2), 380-385 (2010).

[29] Chebaane, M., Bellouz, R., Oumezzine, M., Fouzri, A., Copper-doped lanthanum manganite $La_{0.65}Ce_{0.05}Sr_{0.3}Mn_{1-x}Cu_xO_3$ influence on structural, magnetic and magnetocaloric effects, RSC Advances **8,** 7186-7195 (2018).

[30] Kameli, P., Vaezi, H., Ehsani, M.H., Aslibeiki, B., Salamati, H., Structual, Magnetic, and Transport Properties of $LaMn_{1-x}Cu_xO_3$ (x= 0-0.125) Ceramics, Advanced Ceramics Progress **7** (1), 1-10 (2021).

[31] Kim, M., Yang, J., Medvedeva, J., Yelon, W., Parris, P., James, W., Electronic structure of $La_{0.7}Sr_{0.3}Mn_{1-x}Cu_xO_3$ ($0.0 \le x \le 0.30$), Journal of Physics: Condensed Matter **20,** 255228 (2008).

[32] Kim, M., Yang, J., Cai, Q., Zhou, X., James, W., Yelon, W., Parris, P., Buddhikot, D., Malik, S., The effect of Cu-doping on the magnetic and transport properties of $La_{0.7}Sr_{0.3}MnO_3$, Journal of Applied Physics **97**, 10H714 (2005).